Robot Experiment Analysis of Airport Ramp Area Time Constraints

William J. Coupe * and Dejan Milutinović †
Applied Mathematics and Statistics Department, UC Santa Cruz, CA 95064, USA
Waqar Malik ‡ and Gautam Gupta‡
University of California, Santa Cruz, NASA Ames Research Center, Moffett Field, CA 94035, USA
Yoon Jung §
NASA Ames Research Center, Moffett Field, CA 94035, USA

Improvement in airport operations using optimization schemes has been an active research area in the recent years. Particular attention has been given to improve taxiway and runway queue operations. However, once these operations are improved by an efficient taxiway schedule, its execution relies on the planning of ramp-area aircraft movements. An important step in the integration of the taxiway schedule with the planning of ramp-area aircraft maneuvers is to understand the constraints imposed on the aircraft trajectories due to the geometry of ramp-area and aircraft kinematics. Data for ramp trajectories are usually unavailable. To address this, we use an inexpensive scaled-down robot experiment to collect some critical data about aircraft trajectories. Ramp movement trajectories are then modeled by stochastic processes since they are heavily dependent on the human operator. We use the stochastic model to analyze the relationship between aircraft pushback time intervals and ramp-area conflicts. We then discuss constraints that can be imposed on aircraft pushback intervals to avoid any conflicts among trajectories.

I. Introduction

Airport runways and taxiways have been identified as a bottleneck of the national airspace system (NAS), and the major inhibiting factor for serving an increasing air traffic demand. Since many airports operate at or close to their maximum capacity,[1] an optimization of runway and taxiway operations is necessary. However, once their operations are improved by an optimal taxiway schedule, its execution depends on ramp-area aircraft maneuvers,[2] which is the focus of this paper.

Unlike aircraft maneuvers on taxiways, ramp-area maneuvers are frequently not confined to well-defined aircraft trajectories. The shape and timing of the trajectories are subject to uncertainties resulting from pilots' decisions as well as other factors involved in ramp-area operations, which can impede an optimal taxiway schedule plan. To address this problem, we model the trajectories as stochastic processes. However, ramp-area trajectory data that can be used to build maneuver models are not readily available mainly due to the lack of surveillance data in the ramp-area. Investments in collecting such data are unlikely unless the usefulness of the data in increasing airport efficiency is illustrated. The main goal of this paper is not only to illustrate this, but to point to an inexpensive way to collect the data.

In this paper, we collect the critical data on how a human operator drives aircraft in a ramp area using an inexpensive scaled-down wheeled robot experiment. The use of robots is essential for collecting realistic data because of kinematic imperfections associated with a tolerance in assembly and interaction between the ground and the wheels. This type of uncertainty is reasonable to anticipate with any wheeled vehicle including aircraft. We use E-puck robots[3] and model the movement of aircraft from the gates to the spots in the Terminal C ramp-area of Dallas-Fort Worth International Airport (DFW). The spots are physical areas on the airport surface where the transfer of control from the ramp

*Graduate Student, Applied Mathematics and Statistics Department, UC Santa Cruz.
†Assistant Professor, Applied Mathematics and Statistics Department, UC Santa Cruz.
‡Research Scientist, University Affiliated Research Center, MS 210-8, Moffett Field, CA 94035.
§AIAA senior member and Aerospace Engineer, NASA Ames Research Center, MS 210-6, Moffett Field, CA 94035.

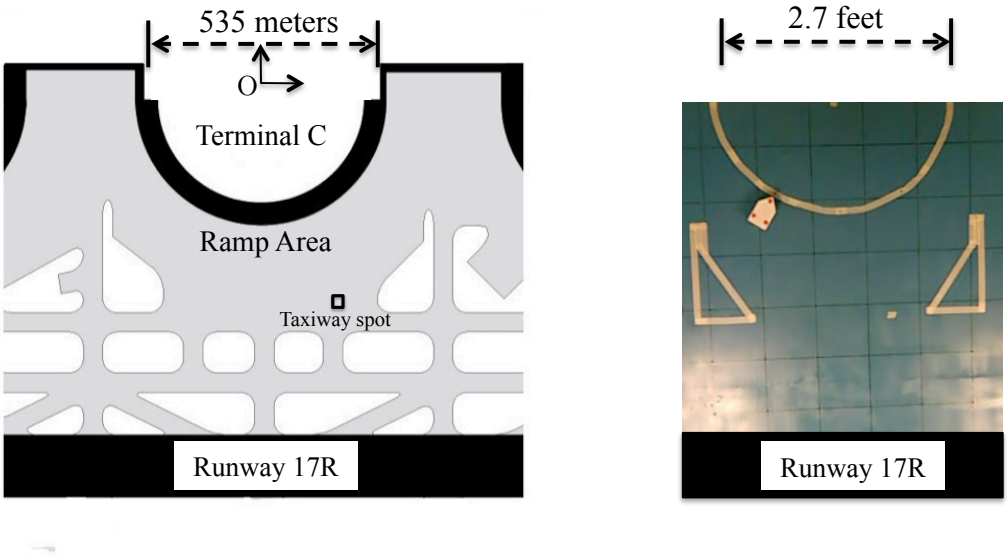

Figure 1. Left panel: Layout of Terminal C at DFW (left); Right panel: scaled-down laboratory model of Terminal C at DFW showing an E-puck robot under a red-dotted lid with three distinctive points helping its tracking, scale is 1 foot = 198 meters (photo from D. Milutinović's Robotics and Control Laboratory, UC Santa Cruz).

controller to the air traffic control tower take place. We assume that a taxiway scheduling plan will be computed by the spot release planner[4] providing us the spot time, which is the concept implemented and tested in NASA's decision support tools for the air traffic controllers (Spot And Runway Departure Advisor –SARDA[2,5]). Therefore, the goal of the analysis is to understand general limitations and trade-offs in the ramp-area scheduling, to provide conflict free movement both in the ramp-area and on taxiway.

Previous work on optimizing airport surface operations has focused on modeling an airport as a graph or a connected network, allowing aircraft to traverse between the nodes along straight edges. The authors used genetic algorithms,[6,7] mixed integer linear programs (MILPs), or hybrids of these.[8,9] The MILP approach has been used in[10–15] and recently also included one form of uncertainties.[16] A more detailed characterization of uncertainties in aircraft taxiing has been considered in,[17] but it only addressed maneuvers in the active movement area (taxiways and runways), and due to unavailability of data it did not tackle the problem in the ramp-area. We are unaware of any work in relation to modeling and planning of maneuvers in the ramp area. To the best of our knowledge this paper is the first attempt to address the integration of a state-of-the-art implementation of an optimal taxiway scheduler, such as SARDA, and ramp area aircraft maneuvers. By using the robot system experiments, we overcome the limitations imposed by the lack of data on ramp operations.

Section II provides a description of the robot experiment that we use to collect our data, while Section III describes our model of aircraft maneuvers. It is followed by Section IV describing our computational analysis based on the model. Results of the computational analysis are summarized by the so-called separation diagram and Section V illustrates the use of ramp area separation graph within SARDA schedulers. Section VI shows that by tailoring aircraft pushback intervals we can decrease the chance of having ramp-area conflicts and illustrates constraints that are used in achieving that decrease.

II. Robot Experiment for Airport Ramp Area Data Collection

The essence of our experiment is in using E-puck robots to obtain estimates of uncertainties of the ramp-area aircraft maneuvers, in particular, the variability of real-life trajectories of pilot driven aircraft. In our experiment, we focus on a single terminal in which a pilot navigates an E-puck simulated Boeing 747 (B747-400) from a designated gate to a taxiway spot.

In this paper, we use a robot experiment with a scaled-down layout of the Terminal C ramp-area of DFW Airport, see Fig. 1. The surface of this scaled-down ramp-area occupies about one half of our 6 ft by 6 ft robotic arena[18] surface. At that scale, the length of a B747[19] is 1.2 times the diameter of the E-puck robot tracked using a ceiling camera. We selected a B747 because the volume it occupies within the ramp-area is larger than the volume of an

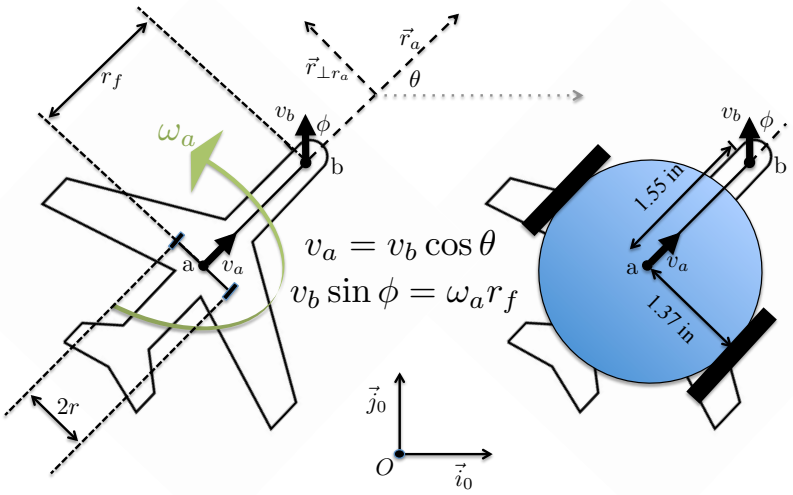

Figure 2. Kinematics characteristics: Boeing 747 (left); E-puck robot (right); v_a - point a (center) velocity; ω_a - angular velocity around the point a (center); v_b - front wheel velocity; ϕ - front wheel angle; θ - the heading angle; r_f - distance between the point a (center) and the front wheel.

average aircraft, as well as because the use of a B747 assumes the turning kinematics and constraints of a large body aircraft, while a smaller aircraft can perform the same maneuvers in a smaller operating space. Therefore, our analysis is conservative with respect to the aircraft size. The slight discrepancy in the dimensions and the major difference in the kinematics between a B747 and an E-puck robot are incorporated in our Tcl/Tk graphical user interface (GUI) for E-puck control, so that an exact match of maneuvers between E-puck and B747 during the pushback and taxi is achieved.

Aircraft kinematics can be modeled as a tricycle[20] with two fixed axis rear wheels and a single front wheel with the controlled steering angle ϕ, see Fig. 2. During pushback, the aircraft motion is powered through the front wheel. Consequently, the pushback variables we control through our Tcl/Tk GUI are the velocity of the front wheel v_b and the angle ϕ. Starting from the tricycle model of the aircraft, we can write

$$v_b\vec{r}_v = v_a\vec{r}_a + (\omega_a r_f)\vec{r}_{\perp\vec{r}_a} \tag{1}$$

where $\vec{r}_v$ is the unit vector pointing in the direction of the front wheel located at b, $\vec{r}_a$ is the unit vector pointing in the direction from a to b, $\vec{r}_{\perp\vec{r}_a}$ is the unit vector that is perpendicular to $\vec{r}_a$, and ω_a is the angular velocity around the point a. From this, we derive two relations between our control variables and the value of the velocities in the points a and b, and the angular velocity around the point a

$$v_b cos\phi = v_a, \quad \omega_a = \frac{v_b sin\phi}{r_f} \tag{2}$$

On the other hand, the control variables for the E-puck motion are velocities of the left (v_L) and the right (v_R) wheels, and their relations to the velocity of the point a on the E-puck (v_a^E) and the corresponding angular velocity (ω_a^E) are

$$v_L = v_a^E - \omega_a^E r, \qquad v_R = v_a^E + \omega_a^E r \tag{3}$$

By setting $v_a^E = v_a$ and $\omega_a^E = \omega_a$, we can derive

$$v_L = v_b cos\phi(1 - \frac{r}{r_f}\tan\phi), \quad v_R = v_b cos\phi(1 + \frac{r}{r_f}\tan\phi) \tag{4}$$

which provides the match between the aircraft and E-puck kinematics, i.e., for our control variables v_b and ϕ, we can compute v_L and v_R so that the E-puck moves in the same way as the aircraft.

At a first glance one may think the pushback and taxi would follow the same model; however, there is a slight difference. While the pushback is powered through a velocity applied at the front wheel $\vec{v}_b$, we can consider that the taxi is powered through a forward velocity applied at the center (point a) of the rear wheels $\vec{v}_a$. Therefore, the control

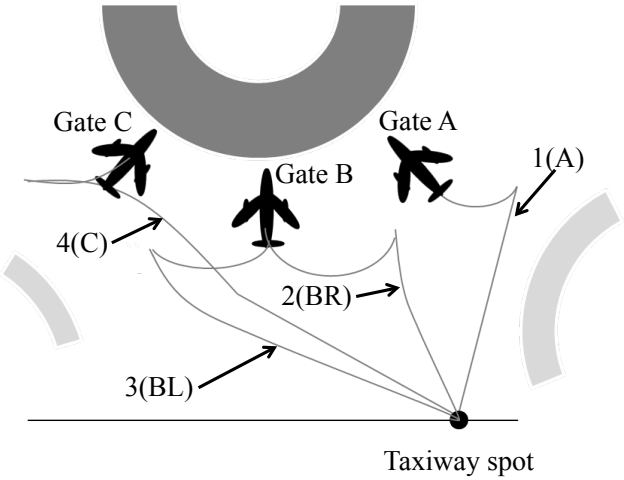

Figure 3. Ramp-area scheduling problem: the aircraft are parked at gates A, B and C, and scheduled to be at the taxiway spot at a given time. The number and letter labels of trajectories provided in brackets are equivalent and used as follows: 1(A) and 4(C) are the trajectories of the aircraft parked at gates A and C, respectively. 2(BR) and 3(BL) are the trajectories of the aircraft parked at gate B, which can push back to the right, or to the left, respectively.

variables we consider are v_a and ϕ. Following similar reasoning as in the pushback case, we find

$$v_L = v_a(1 - \frac{r}{r_f}\tan\phi), \quad v_R = v_a(1 + \frac{r}{r_f}\tan\phi) \tag{5}$$

which are relations providing that for a given forward velocity v_a and the front wheel angle ϕ the E-puck moves the same way as the aircraft, i.e., their kinematics are matched. We can note that the matching of the kinematics in the pushback and taxi modes at any scale depends on the ratio r/r_f, and, in the case of a B747, we have $r/r_f = 0.88$.

Movements of aircraft in the ramp-area are not constrained to well-defined trajectories as illustrated by Fig 3. Upon receiving the pushback clearance, a tug (operated by ground crew) pushes back the aircraft from the gate. At the end of the pushback procedure, the aircraft stops and the tug disengages. This stop period lasts for some time during which the pilot goes through a checklist and then starts the aircraft engine(s). The pilot then taxies the aircraft towards a designated taxiway spot, see Fig.3.

During the maneuvers, the transitions over the motion phases, as well as the path lengths during the pushback and taxi are determined by human operators and are stochastic in nature. In our experiment, the "pilot" drives the E-puck, which moves as if it were an aircraft, using the Tcl/Tk GUI sliders for the steering angle and velocity in the pushback and taxi modes. This provides realistic aircraft motion data. However, we do not know a probability distribution of the time that a real aircraft spend in the stop between the pushback and the forward taxi and this uncertain time has to be inferred from the data. To account for that uncertainty in our experiments, we ask the "pilot" to solve a simple mathematical problem, for example finding eigenvalues of a random 2×2 matrix. Once the "pilot" has solved the problem, he is free to taxi forward towards the taxiway spot.

In order to capture and analyze the data from our experiment, we construct a motion capturing system that works through the use of a general webcam that captures an .AVI video to be processed in MATLAB. We identify 3 points associated with our E-puck and use them to track the position and heading angle of our E-puck. Each individual trajectory is captured providing us with spatio temporal information that includes the uncertainties dues to human operators.

III. Stochastic Model of Aircraft Trajectories

Based on the data captured from our experiment, we model the trajectories of the aircraft pushing back from their gate and taxiing to the spot. We use the model to computationally generate as many trajectories as we need without any further time-consuming robot experiments. This is an important step since our aircraft's conflict-analysis relies on these trajectory samples.

The model describes the trajectories of the aircraft i center (point a, see Fig.2) which starts at the gate, i.e., at the position (x_0^i, y_0^i), and a random heading angle θ^i drawn from the normal distribution $\mathcal{N}(\theta_0^i, (0.18)^2)$ with the mean value θ_0^i and the variance $(0.18)^2$, see Table 1. The trajectories are described based on a hybrid automaton with 5

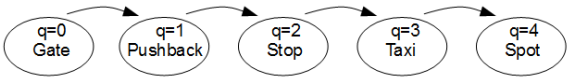

Figure 4. Discrete states of the hybrid automaton model of a ramp-area aircraft trajectory. The states are: 0 - Gate, aircraft is parked at a gate; 1 - Pushback, aircraft pushes back; 2 - Stop, stop after the pushback, 3 - Taxi, taxi towards the taxiway spot, and 4 - Spot, aircraft is at the taxiway spot.

discrete states as shown in Fig. 4 and continuous dynamics as described below with x^i, y^i and θ^i coordinates defined with respect to the global coordinate frame $(\vec{i}_0, \vec{j}_0)$, see Fig. 2.

Each trajectory is initialized with $q = 0$ (Gate) corresponding to the aircraft stopped at the gate. The kinematics in this state, as well as in the states $q = 2$ (Stop) and $q = 4$ (Spot), is defined by

$$dx^i = 0,\ dy^i = 0,\ d\theta^i = 0, \tag{6}$$

In the discrete state $q = 1$ (Pushback), the kinematics is assumed to be deterministic because of small variations in experimentally collected trajectories during that phase of aircraft maneuver, i.e.,

$$dx^i = -v\cos(\theta^i)dt,\ dy^i = -v\sin(\theta^i)dt,\ d\theta^i = -\frac{v}{R^i}dt \tag{7}$$

where the velocity is assumed to be constant $v = 3.5m/s$ and values R^i are provided in Table 1 for every $i = 1,2,3,4$. Finally, the kinematics in the state $q = 3$ is

$$dx^i = v\cos(\theta^i)dt,\ dy = v\sin(\theta^i)dt,\ d\theta = \sigma^i_\theta dW_{\theta^i} \tag{8}$$

where dW_{θ^i} are increments of mutually independent unit intensity Wiener processes and σ^i_θ are their scaling factors, i=1, 2, 3, 4.

All the above mentioned parameters are estimated based on the experimental data and we use the same data to estimate the time distributions of an aircraft in the discrete states $q = 1$ (Pushback), $q = 2$ (Stop) and $q = 3$ (Taxi). These times are modeled by the gamma distributions shown in Fig. 5. We use these distributions and the model in Fig. 4 with kinematics (6)-(8) to generate aircraft trajectories. However, to account for the fact that aircraft maneuver towards the spot, we accept a generated trajectory only if at some terminal time $t = T$, the trajectory belongs to the spot defined as $129 < x^i(T) < 149$, $-537 < y^i(T) < -517$ and $|\theta^i(T) - \pi/2| < 0.326$. [a]

Figure 6 (left) shows a fraction of our experimental data with an E-puck under a red-dotted lid that can be easily tracked in a sequence of video frames. The right panel of the same figure shows our model-generated aircraft trajectories. Note that the model is defined to account for all possible ways aircraft can go from a gate to the spot, therefore the model generated trajectory distributions wider than these may interfere with a tighter fit from experimental data. Having a model that accounts for more possible trajectories makes our analysis more robust against sources of uncertainty of aircraft maneuver trajectories.

IV. Aircraft Trajectory Conflict Analysis

Although the movement of the aircraft in the ramp-area is not constrained to well-defined trajectories and is subject to uncertainties, it is expected that the aircraft reach the spot at specific times provided by the taxiway scheduler; this

[a] In our experiments, the spot is a $20m \times 20m$ area centered at point $(139m, -527m)$, measured from the point O (see Fig. 2) with coordinate $(0m, 0m)$, and with positive directions north for the y coordinate and east for the x coordinate. We do not explicitly constrain how the aircraft approach the spot, but only require that the heading angle of aircraft within the spot at the terminal time T is in the interval $[-\frac{\pi}{2} - 0.326, -\frac{\pi}{2} + 0.326]$.

Table 1. Model parameters for aircraft i trajectory: (x^i_0, y^i_0) - initial aircraft position, θ^i_0 - initial heading angle , R^i - radius of the aircraft trajectory during the pushback, σ^i_θ - scaling factor of the heading angle variations, $[t^i_{S0}, t^i_{F0}]$ - interval in which aircraft i has to push back to be at the spot at $t = 0$.

i	(x^i_0, y^i_0)(m)	$\theta^i_0(^o)$	R^i (m)	σ^i_θ	t^i_{S0}	t^i_{F0}
1 (A)	(151.94, -232.80)	123.13	60	0.051	-162	-102
2 (BR)	(0.00, -278.00)	90	65	0.03	-147	-110
3 (BL)	(0.00, -278.00)	90	60	0.085	-142	-102
4 (C)	(-151.94, -232.80)	56.87	95	0.095	-168	-129

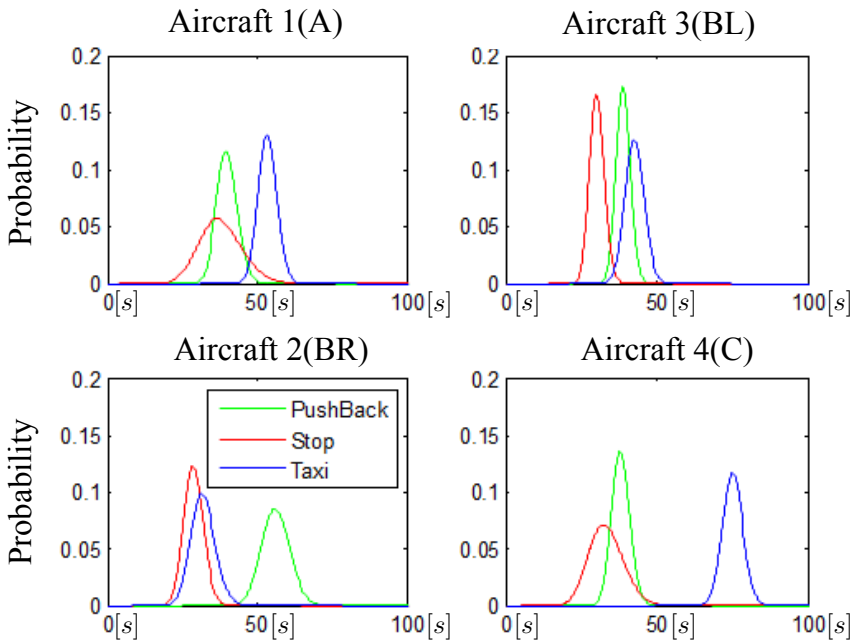

Figure 5. Time distributions of an aircraft in the discrete states: Pushback (green), Stop (red) and Taxi (blue); the time scale presented in seconds

ensures that the aircraft enter the taxiway on-time and without stopping at the spot. For the three aircraft presented in Fig. 3, let us introduce four labels $i = 1,2,3,4$ equivalent to labels A, BR, BL and C that uniquely identify the aircraft and the push back maneuver type. The scheduler provides the spot times t^i_{sch}, but since labels 2 and 3, i.e., BR and BL, correspond to the same aircraft positioned at the gate B that can perform maneuver to the right, or to the left we have $t^2_{sch} = t^3_{sch}$.

Once we are able to generate aircraft trajectories from every gate to the spot, we can calculate the time intervals $[t^i_{S0}, t^i_{F0}]$ when aircraft i has to pushback to reach the spot at $t^i_{sch} = 0$. These values are provided in the last two columns of Table 1. In general, we assume that the terminal time for each trajectory t^i_{sch} is provided by a taxiway scheduler and the corresponding pushback time intervals $[t^i_S,\ t^i_F]$ for achieving t^i_{sch} can be computed as $t^i_S = t^i_{S0} + t^i_{sch}$ and $t^i_F = t^i_{F0} + t^i_{sch}$.

If the difference between two aircraft i and j spot times, i.e., $t^j_{sch} - t^i_{sch}$, is small, then the taxiway scheduler requires the two aircraft to be at the spot within a small time interval. This will likely result in the conflict at the spot. However, the trajectory overlaps in Fig.6 (right) suggest that a conflict may also happen along the paths from gates to the spot.

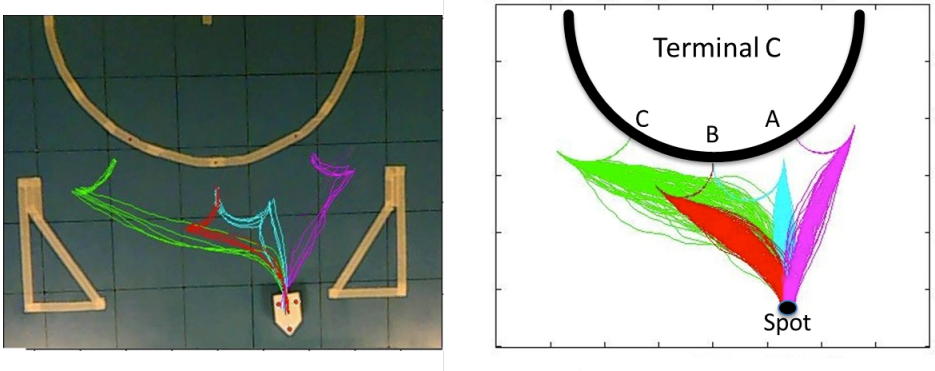

Figure 6. Left panel: a fraction of experimentally recorded trajectories in a layout of the scaled-down ramp-area; Right panel: the model-based generated trajectory samples.

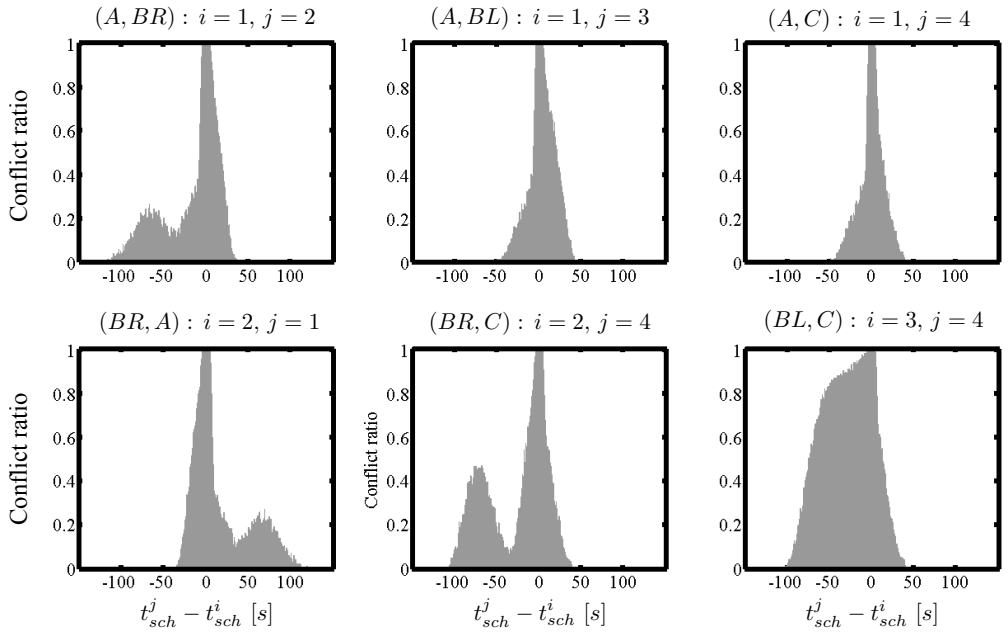

Figure 7. Frequencies of maneuver conflicts against separation times $t^j_{sch} - t^i_{sch}$, $i < j$ at the spot for all aircraft combinations, i.e., gate-spot trajectories taking into account that the aircraft from gate B can perform left (BL) or right (BR) maneuver. Panel BR, A (bottom-left) is a mirror image of distribution A, BR(up-left) and illustrates that distributions for combinations $i > j$ are mirror images of distributions for $i < j$

To get an insight into a possible conflict resolution strategy, we perform the following computational analysis.

Computational analysis: We first take aircraft $i = 1$, i.e., the aircraft at gate A, and assign it the spot time $t^i_{sch} = 0$, therefore its trajectories start at the interval $[t^i_{S0}, t^i_{F0}]$. Then, we take another aircraft, $j = 2$(BR), which starts at gate B and performs the right turn, and assign it t^j_{sch} with a certain negative, or positive value. Therefore, the BR trajectories start at the interval $[t^j_S,\ t^j_F]$. We sample trajectories for these two aircraft, measure their proximity and compute the conflict ratio, i.e., the frequency of trajectory pairs that lose separation. The result for $i = 1$ and $j = 2$ against $t^j_{sch} - t^i_{sch}$ is plotted in the (A, BR) panel of Fig. 7. Clearly, we can repeat the same analysis for $i = 2$(BR) and $j = 1$(A). In this case, we receive the result plotted in (BR, A) panel, which is as expected a mirror image of the previous result. This illustrates that we have to analyze only combinations of i and j such that $i < j$, $i, j = 1, 2, 3, 4$. Moreover, we do not analyze combination $i = 2$(BR), $j = 3$(BL) because both of these two labels are associated with the aircraft from gate B and the labels distinguish the type of its maneuver.

All results of our analysis are presented in Fig. 7. Note that $t^j_{sch} - t^i_{sch} < 0$ means that aircraft i reaches the spot after aircraft j. Similarly, $t^j_{sch} - t^i_{sch} > 0$ means that aircraft i reaches the spot before aircraft j. Therefore, it is not surprising that around $t^j_{sch} - t^i_{sch} = 0$ we have a frequency of conflicts close to 1. We see that some of the distributions are unimodal (A, BL) and (A, C), bimodal (A, BR) and (BR, C), and finally, the distribution (BL, C) seems to be somewhere between these two types of distributions. If the conflict of aircraft maneuvers happens only around the spot, we will have a sharp unimodal distribution. Any other mode of distribution is a consequence of conflicts between aircraft maneuvers along the paths from gates to the spot. The computed diagrams are very useful and can be used to predict the likelihood of conflicts between aircraft for a given separation time at the spot $t^j_{sch} - t^i_{sch}$, or find the separation times providing aircraft maneuvers without conflicts. For example, we can conclude that if $t^2_{sch} - t^1_{sch} > 37$, then there are no conflicts between aircraft 1(A) and 2(BR). The conflict between them does not exist also if $t^2_{sch} - t^1_{sch} < -123$. The negative value means that aircraft 2(BR) reaches the spot at least 123 seconds before aircraft 1(A).

All time separations at the spot providing that aircraft maneuvers are not in conflict can be inferred from Fig. 7 and are summarized by the graph in Fig. 8(a). The graph in Fig. 8(b) is less conservative and shows time separations leading to 10% of conflicts between aircraft menauvers. Each arrow on these graphs points from the aircraft that reaches the spot towards the aircraft that reaches the spot after it. The required separation time is presented above or below each arrow. For example, the graph in Fig. 8(a) shows that to avoid the conflict, aircraft at the gate C executing the only possible maneuver C has to be scheduled to the spot 110s before the aircraft at the gate B performing the right turn maneuver (BR), or 106s before is the gate B aircraft perform the left turn maneuver (BL). If the BR is performed

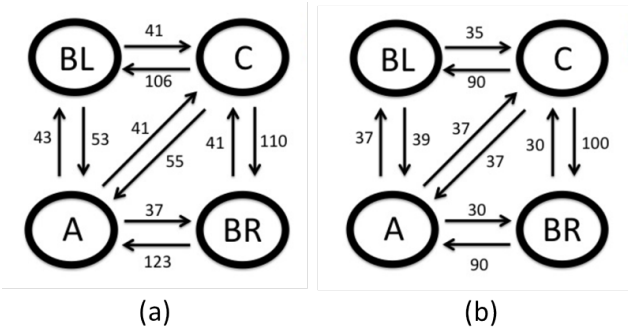

Figure 8. Graphs of time separations (in seconds) at the spot: (a) separations providing 0% of conflict; (b) separations providing 10% of conlfict

then the aircraft at the gate A can be scheduled to the spot 123s, however if BL was performed then the gate A aircraft can be scheduled to the spot 53s after the gate B aircraft.

V. Scheduling Based on the Separation-Time Graph and Integration with SARDA

The graph in Fig. 8(a) captures the results from our aircraft maneuver conflict analysis in section IV. It is a directed graph, $G = (V, E)$, where the edges e_{ij} represent the minimum separation-time that aircraft j can reach the spot after aircraft i to ensure *no* conflict along the path from the gates to the spot. The graph G provides a conservative time-separation at the spot that guarantees conflict-free trajectories. In this section we provide a way to use the graph G in the SARDA scheduler, such that the spot times obtained from the SARDA scheduler guarantee conflict free trajectories in the ramp-areas. Since the spot times calculated in this method already considers the required separations at the spot, it leads to trivial solutions for the gate push-back times. This method is attractive because it provides a simple extension to the Mixed Integer Linear Program (MILP) based runway scheduler for single runway and provides a solution to the surface management problem (conflict-free trajectories for ramp and active movement areas).

A. Spot And Runway Departure Advisor (SARDA)

In this subsection, we provide a brief overview of SARDA's algorithm. SARDA uses the Spot Release Planner (SRP)[4,21] algorithm to provide advisories to the ATCT (Air Traffic Control Tower) controllers. The main idea is to provide spot release advisories to the ground controller (GC) in order to achieve a small queue at the runway and achieve an overall reduction in movement area taxi times. The GC releases the aircraft from the spot at the advised spot-release time and is responsible for maintaining required separations on the taxiway.

The calculation of the optimal spot release involves a two stage algorithm[4]. In the first stage, an optimal runway schedule for the set of aircraft (take-off times for departures and crossing times for arrivals) is generated. For each aircraft, its weight class, and earliest available time at the runway are the main inputs to the SRP algorithm. The earliest available times at the runway are calculated by assuming unimpeded movement of aircraft on the taxiway. The optimization problem of this first stage, formulated as a mixed integer linear program, is given below.

$$min \quad \Gamma := \max_{i \in \mathbb{A}} t_i \tag{9}$$

$$z_{ij} + z_{ji} = 1 \qquad \forall i, j \in \mathbb{A} \tag{10}$$

$$z_{ij}(t_j - t_i - \Delta^r_{ij}) \geq 0 \qquad \forall i, j \in \mathbb{A} \tag{11}$$

$$t_i \geq a_i \qquad \forall i \in \mathbb{A} \tag{12}$$

$$z_{ij} \in \{0, 1\} \qquad \forall i, j \in \mathbb{A}, i \neq j \tag{13}$$

$$t_i \in \mathbb{R}^+ \qquad \forall i \in \mathbb{A} \tag{14}$$

where $\mathbb{A}$ is the set of flights, z_{ij} is a binary variable for relative sequencing of aircraft i and j at the runway, t_i is a continuous variable for the runway usage time for aircraft i. The parameter a_i represents the earliest available time at the runway for aircraft i and Δ^r_{ij} is the minimum required separation-time that aircraft j can *use* the runway after aircraft i. Runway *use* can denote a departure take-off, an arrival landing, or an aircraft crossing the active runway.

The second stage of the SRP determines optimal times to release aircraft from assigned spots to meet departure schedules calculated in the first stage and can be calculated using,

$$t_{is} = t_i - \tau_i, \qquad \forall i \in \text{departures} \tag{15}$$

where τ_i is the unimpeded taxi time for the i^{th} aircraft.

At DFW, once aircraft leave the spots they have specific set of taxi routes to the departure runway. The SARDA simulations[5] considered only East side operations at DFW in south flow configuration with one departure runway ($17R$) and two arrival runways ($17C$ and $17L$). Arrivals landing on $17C$ or $17L$ cross $17R$ at one of the five runway crossing points. The wake-vortex separation between two departures are given in Table 1. Moreover, arrivals can cross runway 17R forty seconds after a departure and they take twenty-one seconds to clear the runway. If two arrivals cross the runway consecutively, the minimum temporal separation between them is five seconds if they are at different crossings, or twenty seconds if they are at the same crossing. Given the minimum separation-time requirements, Δ^r_{ij} for all given pairs of aircraft that use runway $17R$ can be determined.

Table 2. Wake vortex separation (in seconds) for departure aircraft.

	Large	Heavy	B-75x
Large	61	109	91
Heavy	61	90	91
B-75x	61	109	91

B. Incorporating uncertain ramp trajectories in SARDA scheduler

We can decompose the spot separation-time graph G into two subgraphs $G_L = (V_L, E_L)$ and $G_R = (V_R, E_R)$, with $V_L = \{A, BL, C\}$ and $V_R = \{A, BR, C\}$, corresponding to the decision of right/left pushback of aircraft B that we envision to be communicated to the aircraft B prior its pushback from the gate. Without loss of generality, we will use $G^s = (V^s, E^s)$ to interchangeably stand for either G_L or G_R, where $e^s_{ij} \in E^s$ provides the separation-times at the spot for the given pushback (left/right) decision.

DFW airport has a set of structured routes for departures from the spots to the runway. Since aircraft can take different routes to the runway, let us define the parameter δ_{ij} to represent the projected separation at the runway to ensure the required separation at the spot. Given the estimated taxi-time tt_i and tt_j of aircraft i and j respectively, δ_{ij} can be defined as:

$$\delta_{ij} = e^s_{ij} + (tt_j - tt_i)$$

Let $\Delta_{ij} = \max(\Delta^r_{ij}, \delta_{ij})$ be the new required separation between aircraft i and j at the runway. By considering the maximum of the wake-vortex separation and the projected runway separations, we constrain the problem to satisfy the ramp-area constraints in addition to the required runway separations. The modified MILP below provides a solution to the surface management problem (with ramp-area management) in one step. Note that this is achieved using the same number of decision variables as SARDA, and should be computationally comparable.

$$min \quad \Gamma := \max_{i \in \mathbb{A}} t_i \tag{16}$$

$$z_{ij} + z_{ji} = 1 \qquad \forall i, j \in \mathbb{A} \tag{17}$$

$$z_{ij}(t_j - t_i - \Delta_{ij}) \geq 0 \qquad \forall i, j \in \mathbb{A} \tag{18}$$

$$t_i \geq a_i \qquad \forall i \in \mathbb{A} \tag{19}$$

$$z_{ij} \in \{0, 1\} \qquad \forall i, j \in \mathbb{A}, i \neq j \tag{20}$$

$$t_i \in \mathbb{R}^+ \qquad \forall i \in \mathbb{A} \tag{21}$$

The analysis we present here clearly illustrates several things. It allows a preliminary integration of ramp-area constraints directly into SARDA without taking care of specific trajectories in the ramp-area. Using the modified Δ_{ij} does not add any additional variables to the SRP formulation, and is not expected to increase the computation time of the algorithm. By considering separation times with zero probability of conflict we may allow the runway to go under-utilized. If we define the separation time at the spot based on an accepted non-zero level of risk, i.e., based on the graph presented in Fig. 8(b), the throughput can be increased. Any further increase of the throughput has to rely on a more detailed analysis of conflicts between aircraft in the ramp-area, and is discussed in the next section.

VI. Using Conflicting Time Combination Cluster Boundaries for Optimal Conflict Resolution

The analysis in the previous section is based on conflict ratios inferred from samples of the stochastic maneuver trajectories. It is conservative because it is based only on differences in the scheduled time at the spot without taking into account the exact push-back time of each aircraft. In this section, we present results of the computational analysis from Section IV, but this time taking into account specific pushback times.

For an illustration, let us focus on the combination (A, BR), which has a bi-modal conflict ratio distribution, and consider the situation $t^2_{sch} - t^1_{sch} = -70$ when aircraft BR reaches the spot 70 seconds before aircraft A. Assuming that $t^1_{sch} = 0$, we know that the pushback time interval for aircraft A is $[t^1_{S0}, t^1_{F0}]$=[-162 -102] (see Table 1) and that the time interval for aircraft B is shifted for -70, i.e., $[t^2_S t^2_F] = [-217 - 180]$. When we computed the conflict ratio, we used these pushback time intervals. However, in this case, instead of just counting conflicts, we are going to describe all combinations of pushback times that lead to conflicts.

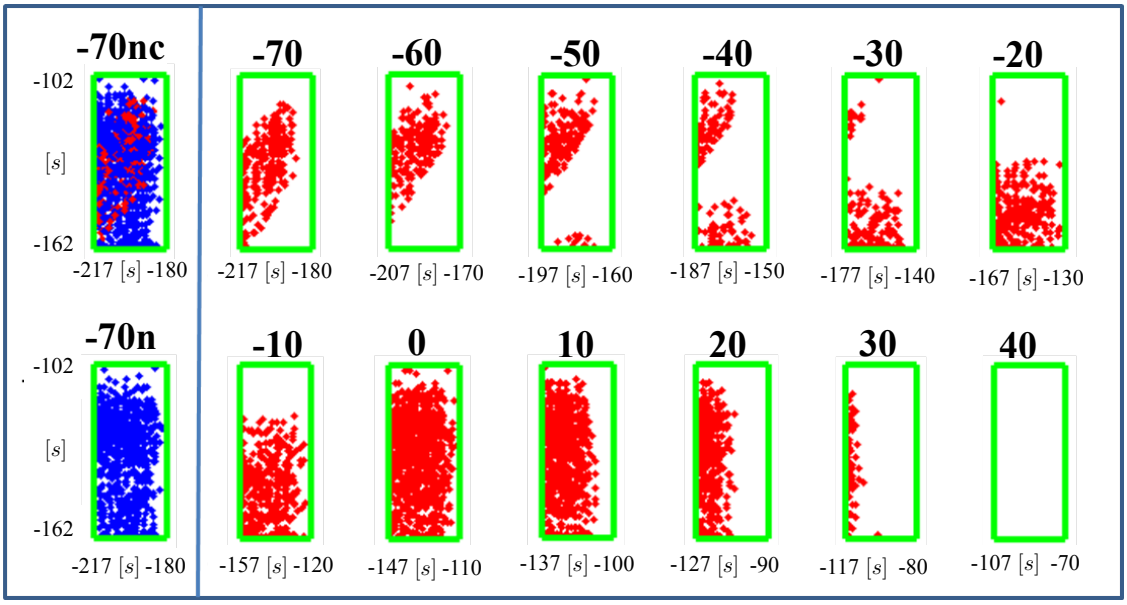

Figure 9. Structure of the conflict between A and BR: Each panel shows the combinations of pushback times for A (vertical axis) and BR (horizontal axis) under the assumption that BR reaches the spot after the time indicated above the panel. The negative values indicate that BR reaches the spot before aircraft A. The panel "-70nc" shows both conflicting and nonconflicting combinations, while "-70n" shows only nonconflicting ones. The corresponding conflicting combinations are presented in the panel "-70". Note that the panel "40" is empty, which means that there are no conflicts.

In Fig. 9, panel "-70nc" (**n**o-conflict and **c**onflict combinations), any time the combination of pushback times results in a conflict, we plot a red dot; otherwise, we plot a blue dot. Although we can distinguish regions containing red, or blue dots, we note that these regions are not well separated by plotting the red and blue dots separately in panels "-70n"(**n**o-coflict combinations) and "-70", respectively. Since we only care about conflict resolution, we focus on modeling the regions in which we find red dots. The panels from "-70" to "40" show the conflict pushback combinations labeled with the difference in time when A and BR aircraft reach the spot.

The shape of conflict zones, i.e., clusters of pushback combinations resulting in maneuver conflicts, is not simple and we can have more than one cluster of pushback combinations in a single diagram, see, for example, Fig. 9 panel "-40". This is likely due to the conflicts along the maneuver paths. For the difference of scheduled time -10 seconds, we know that the conflict happens around the spot and the conflict zone can be bounded by a horizontal line. The shape of the zone says that both aircraft can reach the scheduled time, but the pushback interval for aircraft A has to be narrowed. Otherwise, aircraft A can be too early and in conflict with aircraft B. At the time difference 0 seconds, we have 100% of conflicts as expected and, for the difference of scheduled time of 10 seconds, the conflict zone is limited by a vertical line. In the latter case, aircraft A reaches the spot 10 seconds before aircraft BR. Therefore, the pushback interval of BR has to be narrowed providing that BR is late enough to avoid the conflict with aircraft A.

Next, we examine the detailed conflict zone for $t^1_{sch} - t^2_{sch} = -55$ given in Fig. 10a. The figure shows that if -55 seconds is to be achieved, then a possible option is to take pushback time combination below the line connecting (-202,

-149) and (-165, -116). These pushback times are given by the following inequality

$$t^1 < \frac{-116+149}{-165+202}(t^2+202) - 149 = \frac{33}{37}(-202-t^2) - 149 \tag{22}$$

where in any case $t^2 \in [-202,-165]$. Therefore, a possible combination of pushback time intervals is $[t_S^1 = -162, t_F^1 = -149]$ and $[t_S^2 = -202, t_F^2 = -165]$ resulting in the minimal time interval of 13 seconds for aircraft A and the maximal time interval of 37 seconds for aircraft BR. Figure 10b shows that any extension of the pushback time interval for A leads to a shorter pushback time interval for aircraft BR. Consequently, it makes sense to make a trade-off of the time intervals, so that their minimal length is maximal. In this case, it means that their lengths should be equal. Their limits

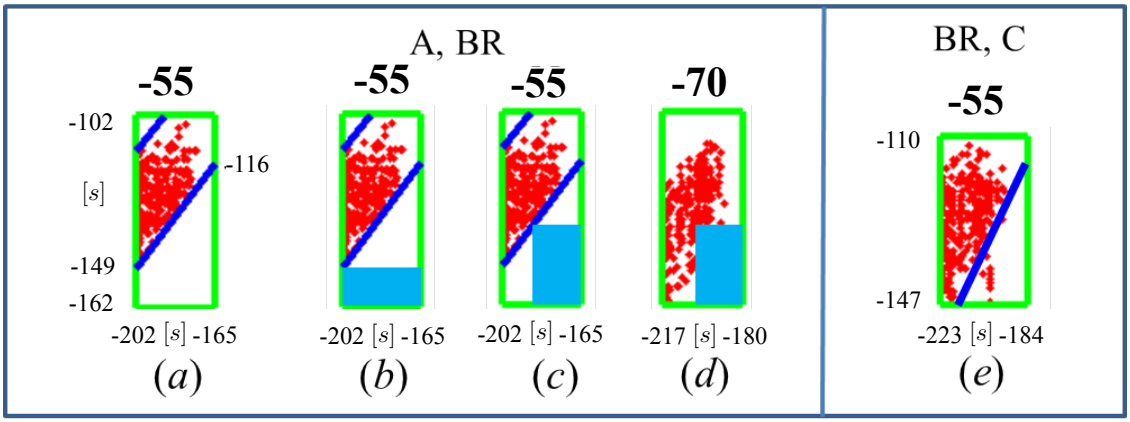

Figure 10. Linear constraints and pushback times for A(vertical axis) and BR (horizontal axis) in the panels (a)-(d) and BR(vertical axis) and C(horizontal axis) in the panel (d): (a) linear constraints bounding the conflicting combinations of pushback times; (b) the full rectangle representing the regions of pushback times providing no conflicts; (c) the full rectangle representing the regions of pushback times providing that the length of time intervals for both aircraft is equal (d) the region of pushback times of the same size as in the panel (c) and its relation to the conflict zone for the time difference at the spot -70; (e) the conflict zone with a possible linear constraint, which does not allow conflict free pushback times. The level of the accepted conflict ratio is 10^{-2}.

are given by $t_S^1 = -162$, $t_F^2 = -165$, while

$$t_F^2 - t_S^2 = \underbrace{\frac{33}{37}(t_S^2+202) - 149}_{t_F^1} - t_S^1 \Rightarrow t_S^2 = -189.3, t_F^1 = -137.7 \tag{23}$$

and, consequently, $t_F^1 - t_S^1 = t_F^2 - t_s^2 = 24.3\ s$. However, note that this length of the pushback time intervals is a valid choice only for the time difference at the spot of -55 and cannot be applied in general. Figure 10*d* shows that if we use the same pushback time interval lengths in the case of the spot time difference of -70, we enter the conflict zone. The example in Fig. 10*e* shows that the region of pushback time combinations leading to conflicts can be more complex, so to keep a linear expression for the pushback time conflict region boundaries, we have to accept a certain nonzero conflict ratio. In the case of the boundary presented in Fig. 10*e*, the level of conflict is 1%, which is likely to be acceptable.

From the analysis of this section, we conclude that: (1) the conflict zones can be composed of more than one cluster of combinations leading to the conflict; (2) these zones can be bounded by linear constraints if we accept a certain level of the conflict, therefore, potentially the constraint can be easily integrated within the SARDA ; finally, (3) the time intervals providing an accepted level of conflicts are specific to the exact value of the aircraft time difference at the spot. This suggests that the control of surface traffic should be organized in such a way that the taxiway scheduler computes t_{sch}^i and the ramp-area maneuver optimization uses the differences among t_{sch}^i to compute pushback time intervals.

VII. Conclusions

In this work, we used the scaled-down robot experiment to provide us the critical trajectory data in the ramp-area, which are not available due to the lack of surveillance data in airport ramp-areas. Based on our robot experiment data and stochastic model for the aircraft trajectories, we can for the first time inspect aircraft pushbask time combinations leading to trajectory conflicts, which are also the result of specific aircraft maneuvers and ramp-area geometry.

We analyzed time constraints to avoid conflicts and developed a time-separation graph at the spot that provided conflict-free ramp-area trajectories. Then, we provided a scheme to use the time-separation graph data within SARDA. While this shows the usefulness of our result, the scheme is conservative, i.e., by providing a conflict-free motion of aircraft, it may lead to the underuse of taxiway. Therefore, we provided a detailed analysis of pushback times leading to conflicts. The analysis shows that sets of conflict-free gate pushback time combination intervals can be formulated based on linear constraints. This means that less conservative time-separation constraints taking into account the ramp-area can be integrated within SARDA.

Now that we understand the type of constraints in the ramp-area, our future work will focus on quantitative methods for generating constraints that we can use in pushback time interval computations, as well as on optimization methods for computing pushback time intervals and integration with SARDA. We also consider important validating our robot experiment data driven analysis against the data from ramp-area operations, for example by comparing the distribution of times that take aircraft from the gate to the spot. In our future work, we would like to consider not only departing, but also arriving aircraft and multiple spots. To that end, we shall work on an upgrade of our experiment to include multiple robots, in which some of the robots will move autonomously to simulate arriving aircraft. Finally, it is worth mentioning that in this work, we used a robot of the size that with respect to the laboratory experiment ramp-area layout dimensions matches the size of a B-747. Since it is a large aircraft, our analysis is conservative with respect to the aircraft size. Collecting data for a smaller aircraft will require either the use of a robot of a smaller size, or a larger dimension of the laboratory ramp-area layout. While there are no obvious obstacles in collecting and using such data from robot experiments, it is likely that the necessity for the data is airport specific.

In a big picture of airport operation optimization, our work indicates the importance of the customization of tools such as SARDA to specific ramp-area layouts. Therefore, our plan is to perform the same experiments and analysis for ramp-areas of other US airports.

References

[1]Gilbo, E. P., "Airport capacity: representation, estimation, optimization," *IEEE Transactions on Control Systems Technology*, Vol. 1, No. 3, 1993, pp. 144–154.

[2]Jung, Y., Hoang, T., Montoya, J., Gupta, G., Malik, W., L., T., and Wang, H., "Performance evaluation of a surface traffic management tool for Dallas/Fort Worth international airport," *9th USA/Europe Air Traffic Management Research and Development Seminar*, 2011, pp. 1–10.

[3]*Website of EPFL education robot*, http://www.e-puck.org/, Access date: July 10, 2013.

[4]Malik, W., Gupta, G., and Jung, Y. C., "Managing departure aircraft release for efficient airport surface operations," *Proceedings of the AIAA Guidance, Navigation, and Control (GNC) Conference*, Toronto, Canada, 2010.

[5]Hayashi, M., Hoang, T., Jung, Y., Gupta, G., Malik, W., and Dulchinos, V., "Usability evaluation of the spot and runway departure advisor (SARDA) concept in a Dallas/Fort Worth airport tower simulation," *Proceedings of the 10th USA/Europe ATM R&D Seminar (ATM2013)*, Chicago, Illinois, 2013.

[6]Pesic, B., Durand, D., and Alliot, J. M., "Aircraft ground traffic optimisation using a genetic algorithm," *Genetic and Evolutionary Computation Conference (GECCO)*, San Francisco, CA, 2001.

[7]Aliot, J. M., Gotteland, J.-P., Durand, N., and Page, E., "Aircraft ground traffic optimization," *4th International Air Traffic management R&D Seminar*, Santa Fe, NM, 2001.

[8]García, J., Berlanda, A., Molina, J., and Casar, J., "Optimization of airport ground operations integrating genetic and dynamic flow management algorithms," *AI Commun*, Vol. 18, 2005, pp. 143–164.

[9]Herrero, J. G., Berlanda, A., Molina, J. M., and Casar, J. R., "Methods for operations planning in airport decision support systems," *Applied Intelligence*, Vol. 22, 2005, pp. 183–206.

[10]Smeltink, J. W., Sooner, M. J., de Waal, P. R., and van der Mei, R. D., "An optimisation model for airport taxi scheduling," *INFORMS Annual Meeting*, 2004.

[11]Marín, A., "Airport management: taxi planning," *Annals of Operations Research*, Vol. 143, 2007, pp. 191–202.

[12]Balakrishnan, H. and Jung, Y., "A framework for coordinated surface operations planning at DFW international airport," *AIAA Guidance, Navigation, and Control Conference (GNC)*, Reston, VA, 2007.

[13]Rathinam, S., Montoya, J., and Jung, Y., "An optimization model for reducing aircraft taxi times at the DFW international airpiort," *26th International Conference of the Aeronautical Sciences*, Ancorage, AK, 2008.

[14]Roling, P. C. and Visser, H. G., "Optimal airport surface traffic planning using mixed-integer linear programming," *International Journal of Aerospace Engineering*, Vol. 2008, 2008, pp. 1–12.

[15]Clare, G. L. and Richards, A. G., "Optimization of taxiway routing and runway scheduling," *IEEE Transactions on Intelligent Transportation Systems*, Vol. 12, No. 4, 2011, pp. 1000–1013.

[16]Anderson, R. and Milutinović, D., "An approach to optimization of airport taxiway scheduling and traversal under uncertainty," *Proceedings of the Institution of Mechanical Engineers, Part G: Journal of Aerospace Engineering*, Vol. 227, No. 2, February 2013, pp. 273–284.

[17]Atkins, S., Brinton, C., and Jung, Y., "Implication of variability in airport surface operations on 4-D trajectory planning," *Proceedings of the 8th AIAA Aviation Technology, Integration, and Operations (ATIO) Conference*, Ancorage, AK, 2008.

[18]LaCara, B., Shyvers, P., Lujan, B., Drake, M., Borja, A., Conover, B., Wu, D., and Teng, L., *Autonomous Hive Mind*, Senior Design Project, Baskin School of Engineering, UC Santa Cruz, 2011.

[19]*747-400/-400ER Document D6-58326-1*, http://www.boeing.com/commercial/airports/747.htm, Access date: July 10, 2013.

[20]Rankin, J., Coetzee, E., Krauskopf, B., and Lowenberg, M., "Bifurcation and stability analysis of aircraft turning on the ground," *AIAA Journal of Guidance, Control, and Dynamics*, Vol. 32, No. 2, March-April 2009, pp. 500–511.

[21]Malik, W., Gupta, G., and Jung, Y. C., "Spot release planner: efficient solution for detailed airport surface traffic optimization," *Proceedings of the AIAA Aviation Technology, Integration, and Operations (ATIO) Conference*, Indianapolis, Indiana, 2012.